ELSEVIER

Polymer 40 (1998) 157–169

polymer

Analysis of the dynamic structure factor for semi-dilute solutions of polyisobutylene

Yoshiyuki Einaga*, Daisuke Karube

Department of Polymer Chemistry, Kyoto University, Kyoto 606-01, Japan

Received 16 January 1998; accepted 20 February 1998

Abstract

The equation for polymer concentration fluctuation derived from Onuki's equations of motion is coupled with Onuki's postulate for the partial stresses generated by concentration fluctuation to formulate the dynamic structure factor $S(q,t)$ [t is time and q the magnitude of the scattering vector]. The actual calculation is made for systems in which the elastic relaxation modulus $L(t)$ is given by a linear combination of n exponential functions. It is shown that the corresponding $S(q,t)$ consists of $n + 1$ exponential functions of time, and that the relative strengths and decay rates of these functions are related by a set of algebraic equations to the diffusion coefficient and cooperative diffusion coefficient, as well as the parameters characterizing $L(t)$. These equations for $n = 2$ are used to analyze dynamic light scattering data on semi-dilute solutions of a polyisobutylene fraction in isoamyl isovalerate (Θ solvent) and n-heptane (good solvent). The results give the instantaneous moduli of the solutions which are well compared with the rubbery plateau moduli from viscoelastic measurements, and the friction coefficients which are identical for both solvents when compared at comparable polymer concentrations.

Keywords: Dynamic light scattering; Dynamic structure factor; Relaxation modulus; Diffusion coefficient; Polyisobutylene; Semidilute polymer solution

1. Introduction

Recent dynamic light scattering (DLS) studies [1–12] on semi-dilute and moderately concentrated polymer solutions have revealed that the dynamic structure factor $S(q,t)$ [t is time and q the magnitude of the scattering vector] for these solutions is multi-modal and may be separated into two parts, usually called fast and slow modes. It has been shown that the characteristic decay time of the slow mode came close to the maximum mechanical relaxation time [1–4,9], and so this mode is usually attributed to the viscoelastic deformation of polymer molecules due to concentration fluctuation. Of great interest are the recent disputes [10,11,13–18], both theoretical and experimental, over the theory of Wang [13,14], which predicts that the slow mode disappears when the polymer and solvent components have identical partial specific volumes. In a companion paper [19], Einaga and Fujita have made clear why Onuki's formulation [16] does not support Wang's prediction, by comparing the differential equations for polymer concentration fluctuation derived from the starting equations of the two theories.

The present paper formulates $S(q,t)$ by coupling the differential equation from Onuki's theory with the postulate that Doi and Onuki [15], and also Onuki [16], proposed for the partial stresses. The actual calculation is carried out for the system whose mechanical relaxation spectrum is represented by an array of n discrete line spectra (n is an arbitrary integer). The derived relations for $n = 2$ are applied to analyze DLS data on semi-dilute solutions of a polyisobutylene (PIB) sample in Θ and good solvents.

2. Theoretical

2.1. Basic equation

The system we consider is an equilibrium isothermal, incompressible binary solution consisting of a pure solvent (component 1) and a monodisperse polymer (component 2). For simplicity, it is assumed that the partial specific volumes, v_1 and v_2, of the components are independent of the composition. The differential equation for δc_2 derived

* Corresponding author.

0032-3861/98/$ - see front matter
PII: S0032-3861(98)00227-4

by Einaga and Fujita [19] from Onuki's equations of motion is

$$\partial\delta c_2/\partial t = D\nabla^2\delta c_2 + (c_{20}v_2/\zeta)\nabla\cdot(\nabla\cdot\delta\sigma_1) - (c_{10}v_1/\zeta)\nabla\cdot(\nabla\delta\sigma_2) \quad (1)$$

where δc_2 is the (mass) concentration fluctuation of component i, $\delta\sigma_i$ the partial stress on component i produced by concentration fluctuations, and ζ the friction coefficient defined by

$$\zeta = c_{10}c_{20}/(\rho_0\Omega) \quad (2)$$

with c_{i0} and ρ_0 the mass concentration of component i and the solution density at equilibrium, respectively, Ω Onsager's phenomenological coefficient, and D the mutual diffusion coefficient. The last quantity is defined by

$$D = c_{10}v_1(\partial\pi/\partial c_2)_{T,p}/\zeta \quad (3)$$

with π the osmotic pressure of the equilibrium solution, T the absolute temperature and p the pressure.

To solve Eq. (1) for δc_2, we need information about $\nabla\cdot\delta\sigma_i$. Although Wang [14,20] insists on his own idea, we proceed here with Onuki's postulate [16] (also Doi and Onuki's [15]), which states that $\delta\sigma_1$ may be neglected and $\delta\sigma_2$ may be related to δu_2, the fluctuation of the local velocity of component 2, by the constitutive equation

$$\nabla\cdot\delta\sigma_2 = \int_0^t L(t-t')\nabla[\nabla\cdot\delta\mathbf{u}_2(\mathbf{t}')]\mathrm{d}\mathbf{t}' \quad (4)$$

Here, $L(t)$ denotes the longitudinal relaxation modulus of the polymer. The mass conservation law for component 2 gives $\partial c_2/\partial t + \nabla\cdot(c_2\mathbf{u}_2) = 0$, where c_2 is the mass concentration of component 2 so that $c_2 = c_{20} + \delta c_2$, and $\mathbf{u}_2$ is the local velocity of component 2. Actually, the latter can be replaced by $\delta\mathbf{u}_2$ since the equilibrium value of $\mathbf{u}_2$ is zero. Thus, it follows for δc_2 sufficiently small as compared with c_{20} that the above mass conservation equation may be replaced by

$$\partial\delta c_2/\partial t = -c_{20}\nabla\cdot\delta\mathbf{u}_2 \quad (5)$$

With this substituted into Eq. (4), we get

$$\nabla\cdot\delta\sigma_2 = -(1/c_{20})\int_0^t L(t-t')\nabla[\partial\delta c_2(t')/\partial t']\mathrm{d}t' \quad (6)$$

Therefore, along with $\delta\sigma_1 = 0$, Eq. (1) gives

$$\partial\delta c_2/\partial t = D\nabla^2\delta c_2 + (v_1c_{10}/c_{20}\zeta)\int_0^t L(t-t')[\nabla^2\partial\delta c_2(t')/\partial t']\mathrm{d}t' \quad (7)$$

This integro-differential equation for $\delta c_2(\mathbf{r},t)$ provides the basis for deriving a theoretical expression for $S(q,t)$.

2.2. Principle

If both sides of Eq. (7) are Fourier transformed first with respect to $\mathbf{r}$ and then with respect to t, we obtain

$$[Dq^2 + i\omega + Cq^2\hat{L}(\omega)]\delta\hat{c}_2(q,\omega) = [1 + Cq^2\hat{L}(\omega)/(i\omega)]\delta\hat{c}_2(q,0) \quad (8)$$

where

$$\delta\hat{c}_2(q,\omega) = \int_0^\infty \exp(-i\omega t)\delta c_2(q,t)\mathrm{d}t \quad (9)$$

$$\hat{L} = i\omega\int_0^\infty \exp(-i\omega t)L(t)\mathrm{d}t \quad (10)$$

$$C = c_{10}v_1/(c_{20}\zeta) \quad (11)$$

with $\delta c_2(q,t)$ being the q component of space Fourier-transformed $\delta c_2(\mathbf{r},t)$.

The definition of the (normalized) dynamic structure factor $S(q,t)$ is

$$S(q,t) = \langle\delta c_2(q,0) * \delta c_2(q,t)\rangle/\langle\delta c_2(q,0) * \delta c_2(q,0)\rangle \quad (12)$$

where * denotes the complex conjugate. Then, according to the Wiener–Khinchin theorem, $\hat{S}(q,\omega)$, the Fourier transform of $S(q,t)$, i.e.

$$\hat{S}(q,\omega) = \int_0^\infty \exp(-i\omega t)S(q,t)\mathrm{d}t \quad (13)$$

is given by

$$\hat{S}(q,\omega) = \langle\delta\hat{c}_2(q,0) * \delta\hat{c}_2(q,\omega)\rangle/\langle\delta\hat{c}_2(q,0) * \delta\hat{c}_2(q,0)\rangle \quad (14)$$

The use of Eq. (8) to calculate the right-hand side of this equation gives

$$\hat{S}(q,\omega) = \frac{1 + C\hat{L}(\omega)q^2/(i\omega)}{Dq^2 + i\omega + C\hat{L}(\omega)q^2} \quad (15)$$

The principle to approach $S(q,t)$ consists of first calculating $\hat{L}(\omega)$ from a given $L(t)$, then determining $\hat{S}(q,\omega)$ by Eq. (15), and finally Fourier inverting it to $S(q,t)$ by Eq. (13).

2.3. Discrete relaxation spectrum

Though not feasible for an arbitrary form of $\hat{L}(\omega)$ or $L(t)$, these operations can be carried through analytically for the prototype case in which the mechanical relaxation spectrum is approximated by an array of discrete line spectra, so that $L(t)$ is represented by

$$L(t) = \sum_{i=1}^{n} L_i \exp(-t/\tau_i) \quad (16)$$

Here, n is an arbitrary positive integer, and L_i and τ_i are the strength and relaxation time for the ith relaxation mode, and the subscript number i is chosen so that $\tau_1 < \tau_2 < \cdots$. The

process and main results of the analytic calculation are summarized in Appendix A. We see that $S(q,t)$ corresponding to $L(t)$ given by Eq. (16) is a linear combination of $n+1$ exponentially decaying functions of time.

In what follows, we focus on the derived relations for $n=2$ and work out how to use them for analyzing experimental $S(q,t)$ data. This restriction to n is made, because in practice, separating a measured $S(q,t)$ curve into more than three exponential functions with accuracy and confidence does not seem easy. As shown below, our $S(q,t)$ data were successfully decomposed into two or three components.

For $n=2$, Eq. (16) gives

$$L(t)=L_1\exp(-t/\tau_1)+L_2\exp(-t/\tau_2) \tag{17}$$

with $\tau_1<\tau_2$, and the corresponding equation for $S(q,t)$ is written as

$$S(q,t)=r_1\exp(-\Gamma_1 t)+r_2\exp(-\Gamma_2 t)+r_3\exp(-\Gamma_3 t) \tag{18}$$

with $\Gamma_1>\Gamma_2>\Gamma_3$. With this choice of the subscript number in mind, we call the first, second and third terms in Eq. (18) the fast, slow and slower modes of $S(q,t)$, respectively. According to Appendix A, the following set of six relations holds among six parameters r_i and $\Gamma_i(i=1,2,3)$, and seven parameters q, D, C, L_i and τ_i $(i=1,2)$:

$$r_1+r_2+r_3=1 \tag{19}$$

$$\Gamma_1+\Gamma_2+\Gamma_3=D_c q^2+\tau_1^{-1}+\tau_2^{-1} \tag{20}$$

$$\Gamma_1\Gamma_2\Gamma_3=Dq^2\tau_1^{-1}\tau_2^{-1} \tag{21}$$

$$\Gamma_1\Gamma_2+\Gamma_2\Gamma_3+\Gamma_3\Gamma_1=[D(\tau_1^{-1}+\tau_2^{-1})+CL_0(\delta_1\tau_2^{-1}+\delta_2\tau_1^{-1})]q^2+\tau_1^{-1}\tau_2^{-1} \tag{22}$$

$$r_1(\Gamma_2+\Gamma_3)+r_2(\Gamma_3+\Gamma_1)+r_3(\Gamma_1+\Gamma_2)=CL_0q^2+\tau_1^{-1}+\tau_2^{-1} \tag{23}$$

$$r_1\Gamma_2\Gamma_3+r_2\Gamma_3\Gamma_1+r_3\Gamma_1\Gamma_2=CL_0(\delta_1\tau_2^{-1}+\delta_2\tau_1^{-1})q^2+\tau_1^{-1}\tau_2^{-1} \tag{24}$$

where

$$L_0=L_1+L_2 \tag{25}$$

$$\delta_i=L_i/L_0 \tag{26}$$

$$D_c=D+CL_0 \tag{27}$$

These equations allow D, C, L_i and $\tau_i(i=1,2)$ to be evaluated when Γ_i and r_i $(i=1,2,3)$ are determined experimentally as functions of q. A practical procedure for the evaluation is as follows.

First, with the Γ_i data as a function of q, $\Gamma_1+\Gamma_2+\Gamma_3$, $\Gamma_1\Gamma_2\Gamma_3$, and $\Gamma_1\Gamma_2+\Gamma_2\Gamma_3+\Gamma_3\Gamma_1$ are calculated and plotted against q^2. According to Eqs. (20)–(22), each of the plots should follow a straight line, and D_c, $\tau_1^{-1}+\tau_2^{-1}$, $D(\tau_1\tau_2)^{-1}$, $D(\tau_1^{-1}+\tau_2^{-1})+CL_0(\delta_1\tau_2^{-1}+\delta_2\tau_1^{-1})$ and $\tau_1^{-1}\tau_2^{-1}$ can be determined from the intercepts and slopes. The results allow D_c, D, τ_1 and τ_2 to be computed separately. However, in practice, it is simpler and more desirable to evaluate D from first cumulant data by use of Eq. (A16) in Appendix A.

If the quantity $c_2(\partial\pi/\partial c_2)_{T,p}$, usually called the osmotic compressibility (or modulus), is denoted here by L_π, then it follows from Eqs. (3) and (11) that

$$D=CL_\pi \tag{28}$$

The value of D is already known, and that of L_π is obtainable from separate thermodynamic measurements including static light scattering, osmometry and sedimentation equilibrium. Hence, C can be evaluated by use of Eq. (28). Once C is known, the friction coefficient ζ is calculable from Eq. (11), and L_0 from Eq. (27) with the aid of the known values of D_c and D. Furthermore, L_1 and L_2 can be evaluated separately, but we do not enter this problem here.

2.4. Limiting forms

The limiting forms of r_i and Γ_i at large and small q derived from the set of Eqs. (19)–(24) deserve attention. At large q, we get

$$\Gamma_1=D_c q^2+(L_1\tau_1^{-1}+L_2\tau_2^{-1})/(L_\pi+L_0)+O(q^{-2}) \tag{29}$$

$$\Gamma_2^{-1}=[1+L_1/(L_\pi+L_0)]\tau_1+O(q^{-2}) \tag{30}$$

$$\Gamma_3^{-1}=[1+(L_2/L_\pi)]\tau_2+O(q^{-2}) \tag{31}$$

$$r_1=D/D_c+O(q^{-2}) \tag{32}$$

$$r_2=L_\pi L_1/(L_\pi+L_0)(L_\pi+L_2)+O(q^{-2}) \tag{33}$$

$$r_3=L_2/(L_\pi+L_2)+O(q^{-2}) \tag{34}$$

Eq. (29) warns that the slope of Γ_1 plotted against q^2 may be equated to D_c only in the region of q^2 large enough so that the plot clearly shows an asymptote. Eqs. (30) and (31) give another warning that the asymptotic values of Γ_2 and Γ_3 at large q^2 may not be equated to τ_1^{-1} and τ_2^{-1}, respectively, because the factors multiplied by τ_1 and τ_2 differ in general from unity.

At small q, we have

$$\Gamma_1=\tau_1^{-1}+CL_1q^2+O(q^4) \tag{35}$$

$$\Gamma_2=\tau_2^{-1}+CL_2q^2+O(q^4) \tag{36}$$

$$\Gamma_3=Dq^2+O(q^4) \tag{37}$$

$$r_1=CL_1\tau_1^2[D+2CL_2\tau_2/(\tau_1-\tau_2)]q^4+0(q^6) \tag{38}$$

$$r_2=CL_2\tau_2^2[D-2CL_1\tau_1/(\tau_1-\tau_2)]q^4+O(q^6) \tag{39}$$

$$r_3=1-CL_0[D(\delta_1\tau_1^2+\delta_2\tau_2^2)+2CL_0\delta_1\delta_2\tau_1\tau_2]q^4+O(q^6) \tag{40}$$

The last three equations indicate that, in the region of small q, all r_i vary in proportion to q^4, so the slower mode dominates $S(q,t)$. Furthermore, comparison between Eqs. (29) and (37) shows that the q^2 dependence of the decay rate moves from the slower mode to the fast mode as q increases.

3. Experimental

3.1. Material

The polyisobutylene (PIB) sample used in this work is a fraction L80-3 separated by fractional precipitation with benzene and methanol from a commercial product L-80 of Enjay Chemical Co. Its weight-average molecular weight M_w determined in n-heptane at 25.0°C using a Fica50 light scattering photometer was 8.15×10^5, and the ratio of M_w to the number-average molecular weight estimated by analytical gel permeation chromatography was 1.24.

Isoamyl isovalerate (IAIV, Tokyo Kasei Kogyo), used as a Θ solvent, and n-heptane, used as a good solvent, were purified by standard methods.

3.2. Dynamic light scattering

DLS measurements were made using a Brookhaven Instruments Model BI-200SM light scattering goniometer and vertically polarized incident light of 488 nm wavelength from a Spectra-Physics Model 2020 argon ion laser source equipped with a Model 583 temperature-stabilized etalon for single-frequency-mode operation. The photomultiplier tube was an EMI 9863B/350, and the output was processed by a Brookhaven Instruments Model BI2030AT autocorrelator with 264 channels. The normalized autocorrelation function $g^{(2)}(t)$ of scattered light intensity $I(t)$ was determined at scattering angles θ ranging from 30 to 150°, and was converted to the field correlation function $g^{(1)}(t)$, which is equivalent to our $S(q,t)$, by use of the familiar relation

$$g^{(2)}(t) = 1 + f|g^{(1)}(t)|^2 \tag{41}$$

where f is a constant depending on the optical system used and can be determined by using the property $\lim_{t \to 0} g^{(1)}(t) \to 1$.

The discussion made in the Theoretical section premises that a set of measured $S(q,t)$ at given q can be decomposed into the sum of exponential functions of time. Thus, we attempted the decomposition by utilizing Tobolsky's 'procedure X' [21] familiar in the determination of mechanical relaxation spectra, and found that all of our $S(q,t)$ data were successfully separated into two or three exponential functions, as illustrated below.

DLS measurements were made on two IAIV solutions (A and B) and one n-heptane solution (C). The polymer mass concentrations c ($= c_{20}$ in the Theoretical section) were 0.0297 and 0.0478 g/cm^3 for A and B, respectively, and

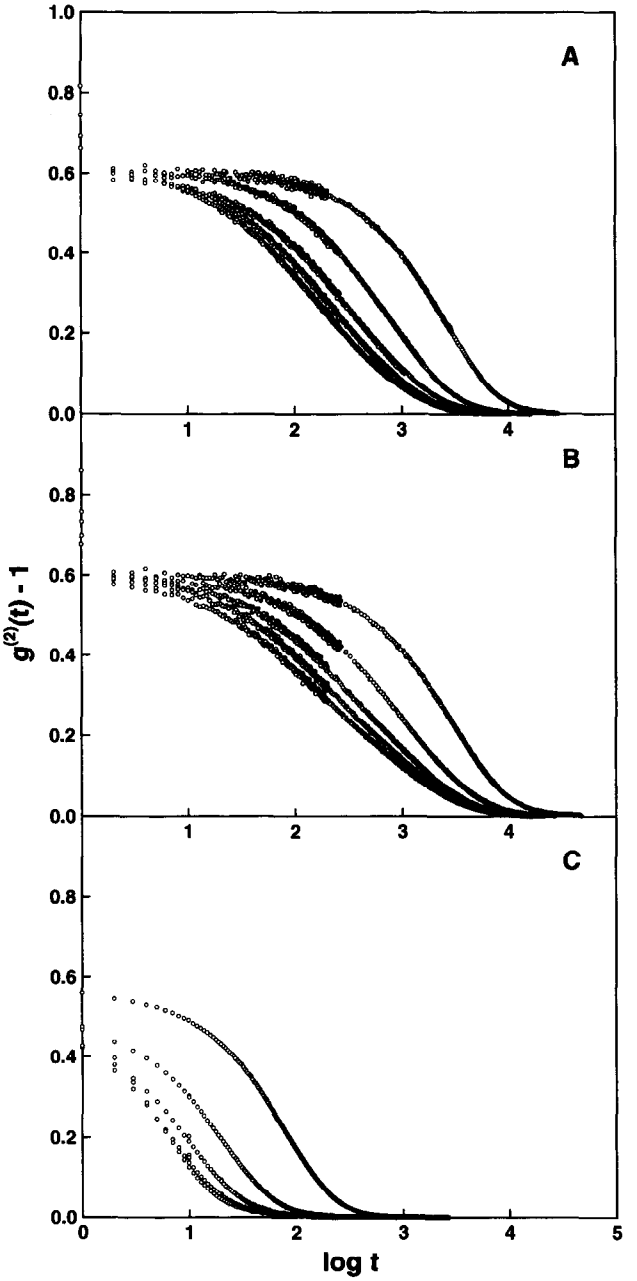

Fig. 1. Plots of $g^{(2)}(t) - 1$ against log t for solutions A, B and C at various scattering angles θ: θ is 30, 60, 90, 120 and 150° from right to left, respectively.

that for C was 0.0445 g/cm^3. At these concentrations, the polymer chains in the solution are well entangled, because $cM_w/(\rho_2^0 M_c)$, a measure of the existence of entanglement, is 1.8 and 2.8 for A and B, respectively, and 2.6 for C. Here, ρ_2^0 is the density of pure polymer and M_c the critical molecular weight for the onset of the entanglement effect on viscosity for pure polymer ($\rho_2^0 = 0.9169$ g cm^{-3} and $M_c = ca.$ 15 000 for PIB) [22,23]. The measuring temperature was fixed at 25.0°C, which is the Θ temperature for the system PIB/IAIV.

To prepare the test solution, a dilute solution of the PIB sample in cyclohexane was filtered into an optically cleaned

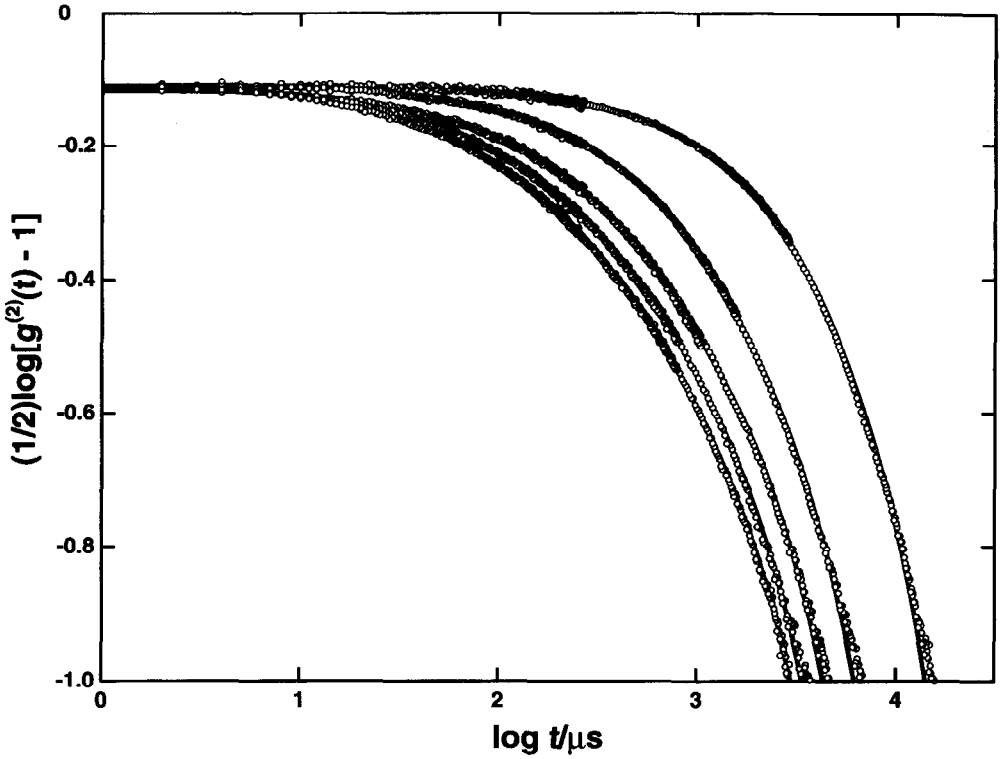

Fig. 2. Plots of $(1/2)\log[g^{(2)}(t) - 1]$ against $\log t$ for solution A ($c = 0.0297$ g cm^{-3}) at various scattering angles θ: θ is 30, 60, 90, 120 and 150° from right to left, respectively. The solid curves indicate the calculated values (see text).

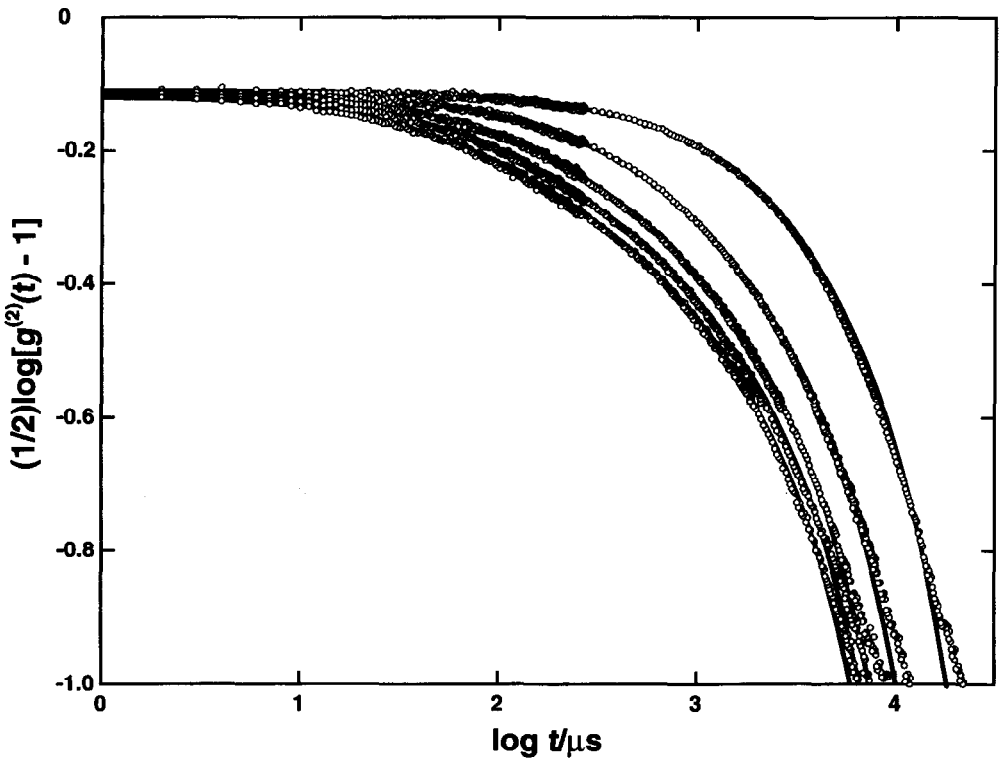

Fig. 3. Plots of $(1/2)\log[g^{(2)}(t) - 1]$ against $\log t$ for solution B ($c = 0.0478$ g cm^{-3}) at various scattering angles θ : θ is 30, 60, 90, 120 and 150° from right to left, respectively. The solid curves indicate the calculated values (see text).

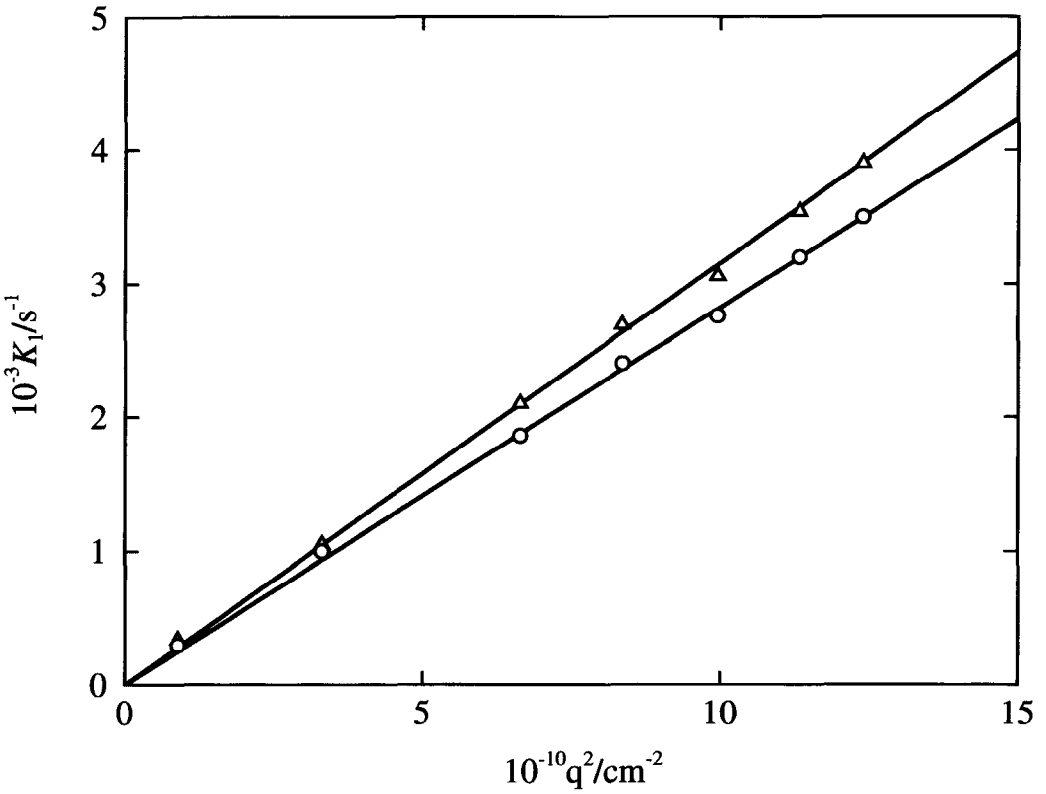

Fig. 4. Plots of K_1 against q^2 for solutions A (triangles) and B (unfilled circles).

light scattering cell with a Teflon membrane of 0.45 μm pore size. The solution was freeze-dried after the cell was covered with a Teflon membrane of the same pore size. Then, an appropriate amount of filtered solvent IAIV or *n*-heptane was poured into the cell. After the cell was tightly sealed, the solution was made homogeneous keeping the cell for 10–14 days at *ca.* 50°C for IAIV and room temperature for *n*-heptane. The value of c was calculated by iteration from the measured weight fraction of the polymer, and the solution density ρ_0 calculated using the published relations at 25°C [24,25]

$$\rho_0 = 0.85066 + 0.0737c \text{ (PIB/IAIV)} \quad (42)$$

$$\rho_0 = 0.67961 + 0.237c + 0.11c^2 \text{ (PIB/}n\text{-heptane)} \quad (43)$$

These can also be used to compute the partial specific volumes v_1 and v_2.

4. Results and discussion

4.1. PIB in IAIV

In Fig. 1, the raw data of $g^{(2)}(t) - 1$ for solutions A and B are plotted against log t, along with those for solution C. It is seen that the data points at each scattering angle determined with different sampling time intervals make a single composite curve, which smoothly tends to approach a horizontal line given by $g^{(2)} - 1 = 0$.

Figs. 2 and 3 depict double logarithmic plots of $[g^{(2)} - 1]^{1/2}$ *versus* t, each referring to θ different by 30°, for solutions A and B, respectively. By virtue of Eq. (41), these data may be viewed as representing the behaviour $f^{1/2}g^{(1)}$ or $S(q,t)$ multiplied by a constant. Although the fast and slow modes are not separately visible in them, the point is that none of them can be fitted by a single exponential function. In other words, they consist of a fast mode, and one or more slow modes.

Fig. 4 shows the first cumulant K_1 for either solution A (triangles) or B (unfilled circles) plotted against q^2, where $q = 4\pi n_0 \sin(\theta/2)/\lambda_0$ with n_0 being the refractive index of the solvent and λ_0 the wavelength of the incident light in vacuum. As expected from Eq. (A16), the data points for each solution fall on a straight line. This implies that the system's mechanical relaxation times τ_i are all longer than 1 μs, the smallest sampling time interval used for our DLS measurements, or that the relaxation moduli with τ_i shorter than 1 μs make no contribution to measured $S(q,t)$. The slopes of the straight lines in Fig. 4 give $D = 3.1_8 \times 10^{-8}$ and $2.8_2 \times 10^{-8}$ cm^2 s^{-1} for solutions A and B, respectively. The corresponding friction coefficients ζ are computed from the relation

$$D = (1 - cv_2)L_\pi/(c\zeta) \quad (44)$$

which is derived from Eq. (3) with the definition for the osmotic compressibility L_π taken into account. We used $v_2 = 0.931$ cm^{-3} g^{-1} obtained from Eq. (42) and

Table 1
Values of the parameters on diffusion and viscoelasticity for polyisobutylene L80-3 ($M_w = 8.15 \times 10^5$) solutions

Solution (c/g cm^{-3})	IAIV, 25.0°C(Θ) A (0.0297)	B (0.0478)	n-Heptane, 25.0°C C (0.0445)
D/cm^2 s^{-1}	$3.1_6 \times 10^{-8}$	$2.8_2 \times 10^{-8}$	$7.4_6 \times 10^{-7}$
ζ/dyne s cm^{-1}	$1.7_8 \times 10^{12}$	$3.9_5 \times 10^{12}$	$3.9_6 \times 10^{12}$
D_c/cm^2 s^{-1}	$7.0_0 \times 10^{-8}$	$8.4_4 \times 10^{-8}$	$8.1_4 \times 10^{-7}$
L_0/dyne cm^{-2}	2.1×10^3	1.1×10^4	1.3×10^4
τ_1/s	1.2×10^{-4}	1.5×10^{-4}	1.8×10^{-5}
τ_2/s	2.1×10^{-3}	3.1×10^{-3}	4.6×10^{-4}
L_1/dyne cm^{-2}	1.8×10^3	8.9×10^3	
L_2/dyne cm^{-2}	2.9×10^2	2.3×10^3	

calculated L_π from

$$L_\pi = cRT(M_w^{-1} + 2A_2c + 3A_3c^2) \quad (45)$$

with Akasaka et al.'s data [24] of A_2 (second virial coefficient) $= -0.8 \times 10^{-5}$ mol $-$ cm^3 g^{-2} and A_3 (third virial coefficient) $= 6.3 \times 10^{-4}$ mol $-$ cm^6 g^{-3} for a PIB sample with $M_w = 8.72 \times 10^5$. The results are summarized in Table 1.

Fig. 5 illustrates the application of the procedure X to the data for solution A at $\theta = 150°$. It is seen that the data are separated into three exponential functions with fair accuracy. We obtained similar success for both A and B at all θ studied, and were able to determine r_i and $\Gamma_i (i = 1,2,3)$ for these solutions as functions of q. Before going further with these results, some comments may be in order.

First, though hardly visible on the semi-logarithmic plots in Fig. 1, the double-logarithmic plots in Figs 2 and 3 reveal wild scattering of the data points in the region of large t, more appreciable at smaller θ. Undoubtedly, this was due to the presence of dust particles in the test solutions, which we failed to remove. Thus, we intentionally discarded such scattered data points in applying the procedure X, but it is certain that this manipulation made our determination of the slower mode of $S(q,t)$ less accurate.

Second, since the procedure X separates the modes from slower to faster decay rate in stepwise fashion, the resulting values of r_1 and Γ_1 unavoidably suffer cumulative errors and are hence less reliable. Therefore, we calculated r_1 and Γ_1 from Eq. (19), and $K_1 = r_1\Gamma_1 + r_2\Gamma_2 + r_3\Gamma_3$ with the known values of Γ_2, Γ_3, r_2, r_3 and K_1. This latter relation can be derived from Eq. (19), Eq. (20) and Eq. (23). The

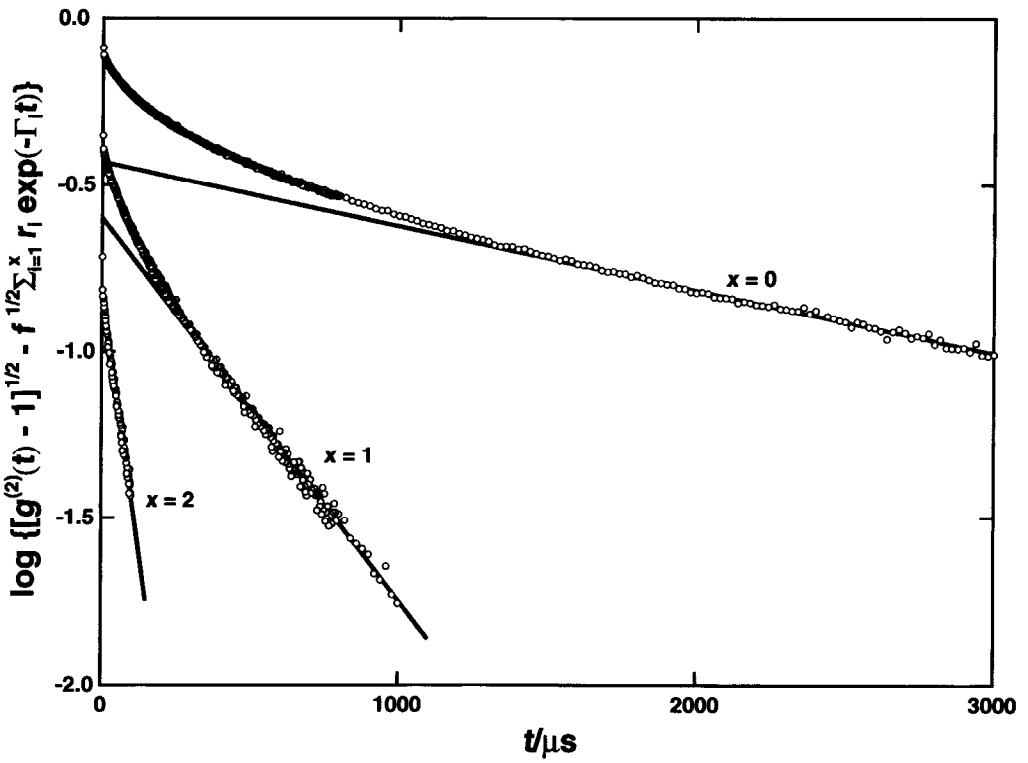

Fig. 5. An example of the procedure X for the results for solution A at $\theta = 150°$. The solid straight lines designated as x = 0, 1 and 2 represent the values calculated by $f^{1/2} r_i \exp(-\Gamma_i t)$ with $i = 1$, 2 and 3, respectively.

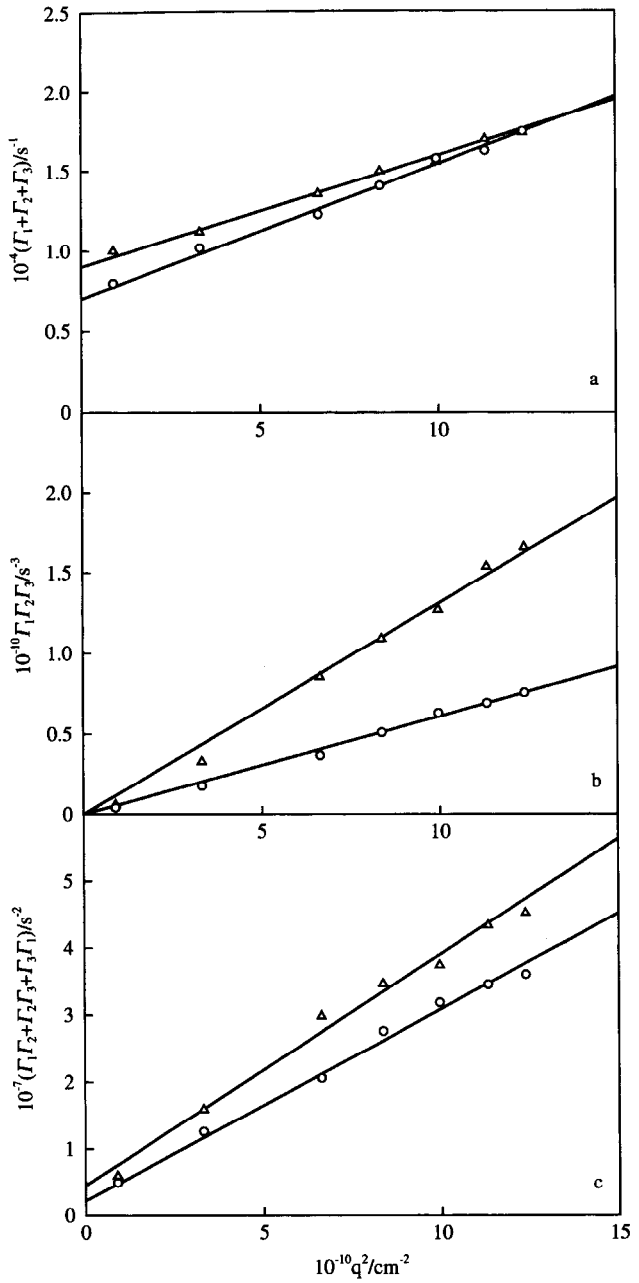

Fig. 6. Plots of $\Gamma_1+\Gamma_2+\Gamma_3$ (a), $\Gamma_1\Gamma_2\Gamma_3$ (b) and $\Gamma_1\Gamma_2+\Gamma_2\Gamma_3+\Gamma_3\Gamma_1$ (c) against q^2 for solutions A (triangles) and B (unfilled circles).

solid curves in Figs 2 and 3, though not clearly seen, have been calculated from Eq. (18) with the values of r_i and Γ_i so evaluated. Their good agreement with data points justifies our data analysis, but does not always warrant that the measured $S(q,t)$ consists of exactly three exponential functions.

Third, one may argue that $[g^{(2)}(t)-1]^{1/2}$ data are more conveniently analyzed with a computer program [3,4,26,27] for Laplace transformation to determine the distribution function $r(\Gamma)$ defined by

$$[g^{(2)}(t)-1]^{1/2}=f^{1/2}\int_0^\infty r(\Gamma)\exp(-\Gamma t)\mathrm{d}\Gamma \qquad (46)$$

However, as far as we are aware, no method to extract information about $L(t)$ from $r(\Gamma)$ is as yet established, and the same can be said of the case in which $[g^{(2)}(t)-1]^{1/2}$ data are fitted by a linear combination of stretched exponential functions [4,11].

Tests of Eqs. (20)–(22) are presented in Fig. 6. We see that our experimental data well obey the q^2 dependence predicted by these equations. The values of the parameters D_c, L_0, L_1, L_2, τ_1 and τ_2 calculated from the indicated straight lines by the method described in the Theoretical section are listed in Table 1, along with those of D mentioned above.

4.2. PIB in n-heptane

Fig. 7 shows $g^{(2)}(t)-1$ data for solution C at five θ. All data for this solution were also successfully separated into three exponential functions by the procedure X, except at $\theta = 30°$ where we had to be content with two exponential functions, owing to the appreciable scattering of the data points in the region of large t. The solid curves, calculated from Eq. (18) with the values of r_i and Γ_i determined, again show good fit to the data points.

Fig. 8 plots K_1 for solution C against q^2. The straight line drawn gives $D = 7.4_8 \times 10^{-7}\,\mathrm{cm^2/s}$, which together with $v_2 = 1.046\,\mathrm{cm^3/g}$ from Eq. (43) and the value of L_π computed by using Akasaka et al.'s data [25] of $A_2 = 2.42 \times 10^{-4}\,\mathrm{mol-cm^3/g^2}$ and $A_3 = 1.74 \times 10^{-2}\,\mathrm{mol-cm^6/g^3}$ for a PIB sample with $M_w = 8.90 \times 10^5$, gives the value of ζ given in Table 1.

Fig. 9 presents tests of Eqs. (20)–(22) for solution C. The predicted q^2 dependence is well substantiated experimentally in all cases. The indicated straight lines lead to the values of D_c, L_0, τ_1 and τ_2 listed in Table 1. For solution C, L_1/L_0 was too small to be estimated accurately.

4.3. Predictability of mechanical properties

We now take a look at the numerical values in Table 1. First, L_0 is comparable for solutions B and C, whose concentrations are close. This finding is reasonable, because L_0 in the present context may correspond to the rubbery plateau longitudinal modulus $L_N(c)$ which is known to be usually independent of solvent species. If the rubbery plateau shear modulus $G_N(c)$ obeys the familiar relation $G_N(c) = G_N^0(c/\rho_2^0)$ [2,28], where the superscript 0 refers to the undiluted polymer, we obtain, with $G_N^0 = 3.2 \times 10^6\,\mathrm{dynes/cm^2}$ for PIB [29], $(4/3)G_N(c) = 4.5 \times 10^3$, 1.2×10^4 and $1.0 \times 10^4\,\mathrm{dynes/cm^2}$ for solutions A, B and C, respectively. While $(4/3)G_N(c)$ for solution A is about twice as large as L_0, those for solutions B and C come close to L_0. This finding implies that the method described in the Theoretical section is capable of estimating the rubbery elastic moduli of entangled polymer solutions approximately from measurements of $S(q,t)$. However, we must remark that it does not always justify the fundamental

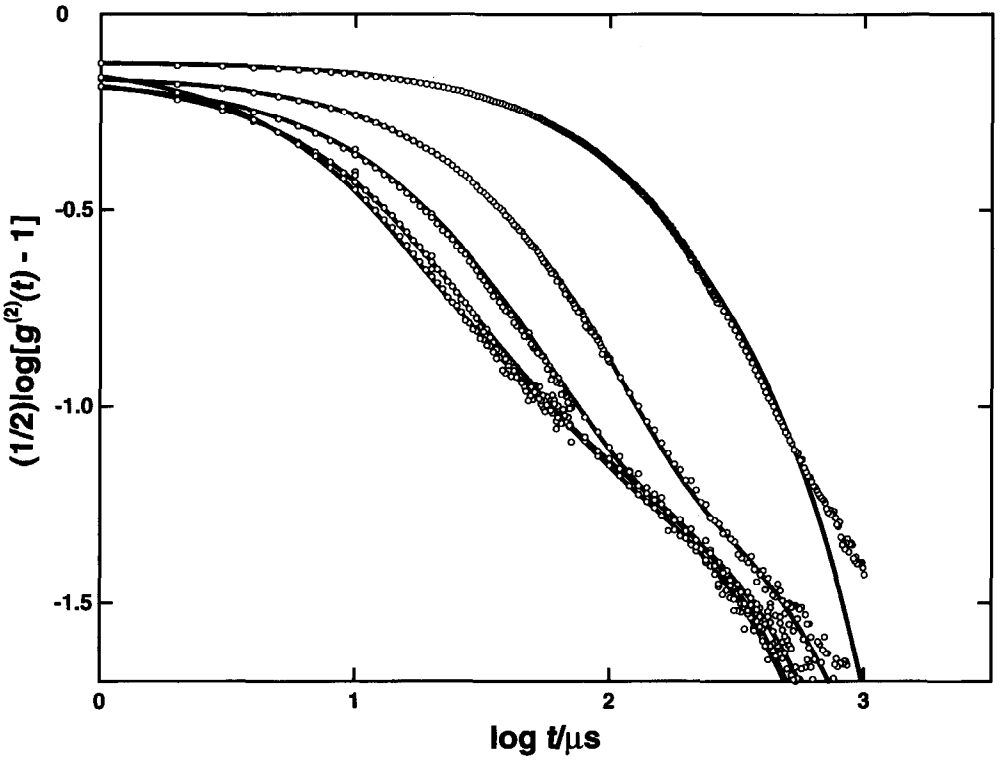

Fig. 7. Plots of $(1/2)\log[g^{(2)}(t) - 1]$ against $\log t$ for solution C ($c = 0.0445$ g cm^{-3}) at various scattering angles θ : θ is 30, 60, 90, 120 and 150° from right to left, respectively. The solid curves indicate the calculated values (see text).

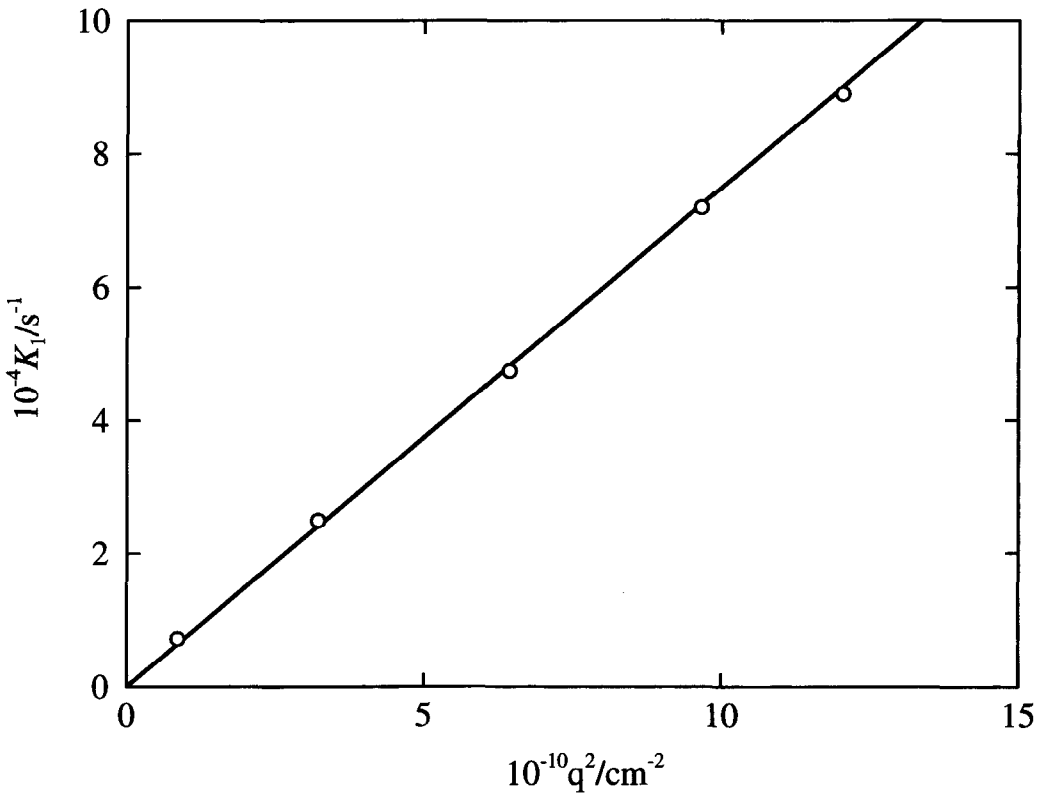

Fig. 8. Plots of K_1 against q^2 for solution C.

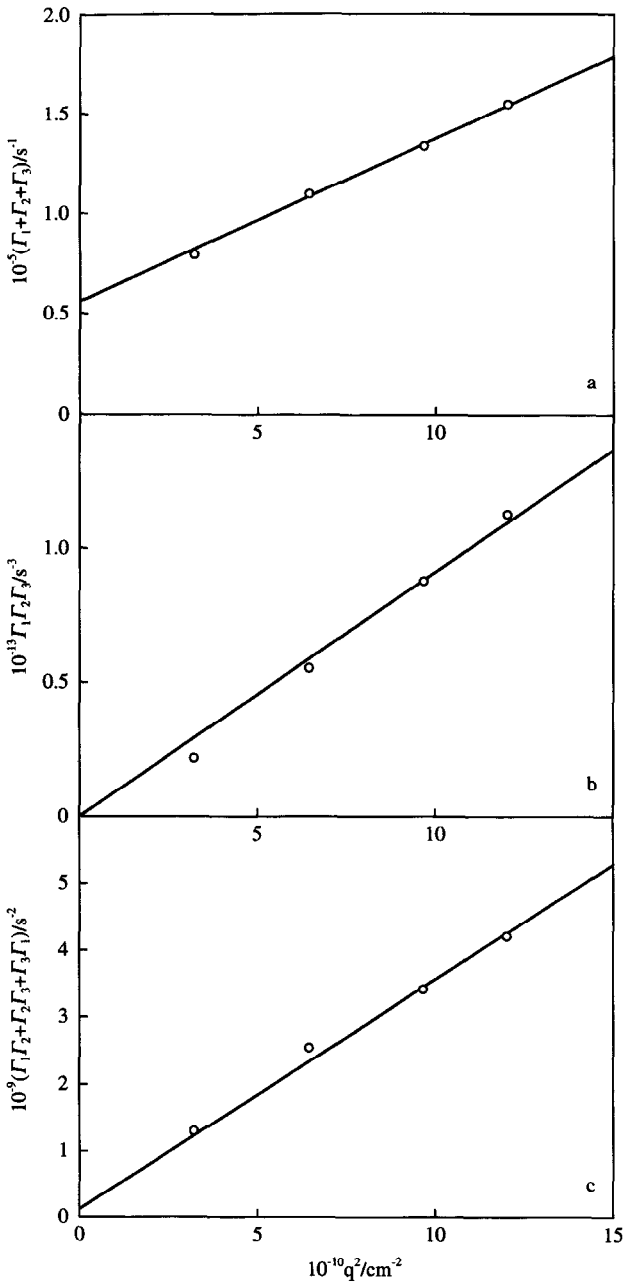

Fig. 9. Plots of $\Gamma_1+\Gamma_2+\Gamma_3$ (a), $\Gamma_1\Gamma_2\Gamma_3$ (b) and $\Gamma_1\Gamma_2+\Gamma_2\Gamma_3+\Gamma_3\Gamma_1$ (c) against q^2 for solution C.

assumption of our theoretical development, i.e. the use of Onuki's postulate for the partial stresses.

The values of ζ for solutions B and C happen to agree, despite a great difference in viscosity η_0 between their solvents (i.e. η_0 of IAIV and *n*-heptane at 25°C are 0.0133 and 0.003902 poise, respectively). This seemingly surprising finding may help understand the factors controlling the friction in entangled polymer solutions.

Finally, Fig. 10 shows the decay rate Γ_1 of the fast mode plotted against q^2, while Figs 11 and 12 show the strength r_1

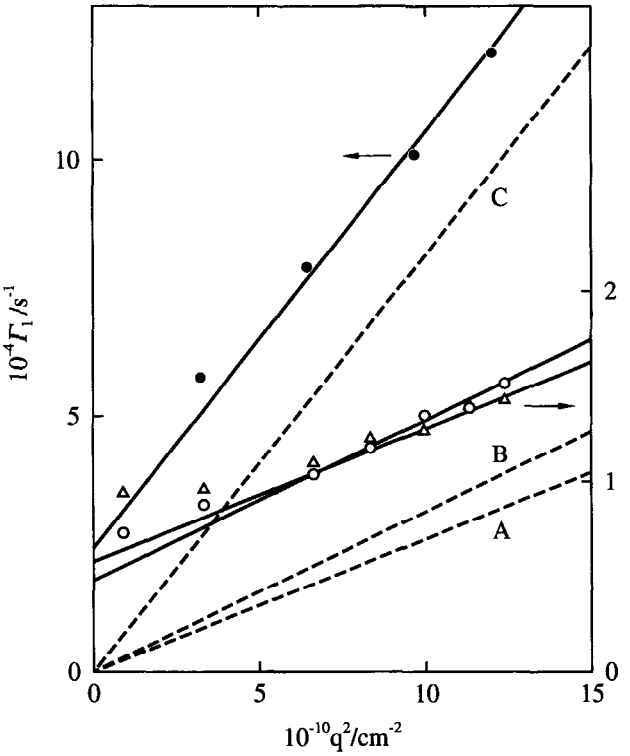

Fig. 10. Plots of Γ_1 against q^2 for solutions A (triangles), B (unfilled circles) and C (filled circles). The dashed straight lines A, B and C represent the relation $\Gamma_1 = D_c q^2$ for solutions A, B and C, respectively, and the solid lines are drawn parallel to the corresponding dashed lines so as to fit the data points at large q^2 values.

of the fast mode and the inverse decay rate Γ_3^{-1} of the slower mode plotted against q^{-2}, for solutions A, B and C. As q^2 increases, the set of data points for each solution in Fig. 10 appears to be fitted by a solid line parallel to the broken line, representing the first term in Eq. (29), i.e. $\Gamma_1 = D_c q^2$. Thus, the solid line is the asymptote for Γ_1 at large q^2, and its correct determination is essential for the right evaluation of D_c. The great deviation of the asymptote from the corresponding broken line is remarkable, indicating that the second term in Eq. (29) plays a significant role in the range of q accessible to DLS measurements. In Figs 11 and 12, where the points on the ordinate axis represent the calculated values of the first term in Eq. (30) or Eq. (31), we see that r_1 strongly depends on q at large q, but less at small q, while the q dependence of Γ_3 is relatively mild over a wide range of q. The behaviour of r_1 suggests that the second term in Eq. (31) is important in the experimentally accessible range of q.

Acknowledgements

We are indebted to Dr Hiroshi Fujita, Professor Emeritus of Osaka University, who helped us in preparing the manuscript of this paper.

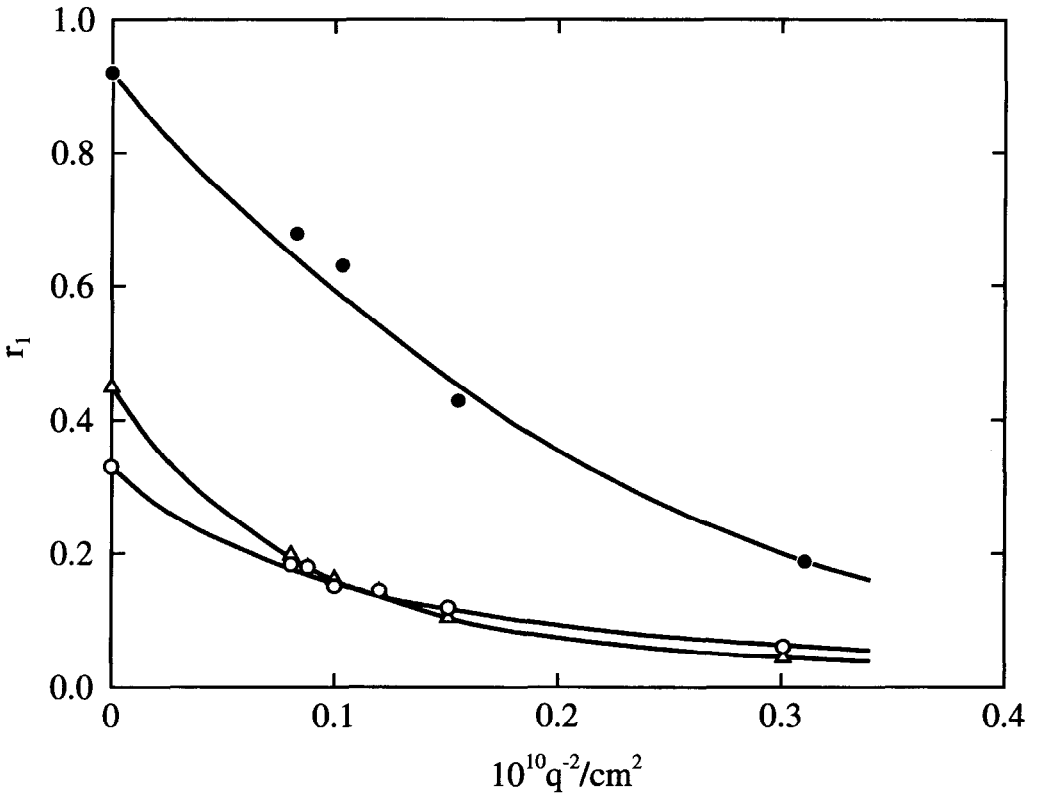

Fig. 11. Plots of r_1 against q^{-2} for solutions A (triangles), B (unfilled circles) and C (filled circles). The data points on the ordinate axis represent the values of $L_\pi/(L_\pi + L_0)$. The solid curves are merely to guide the eye.

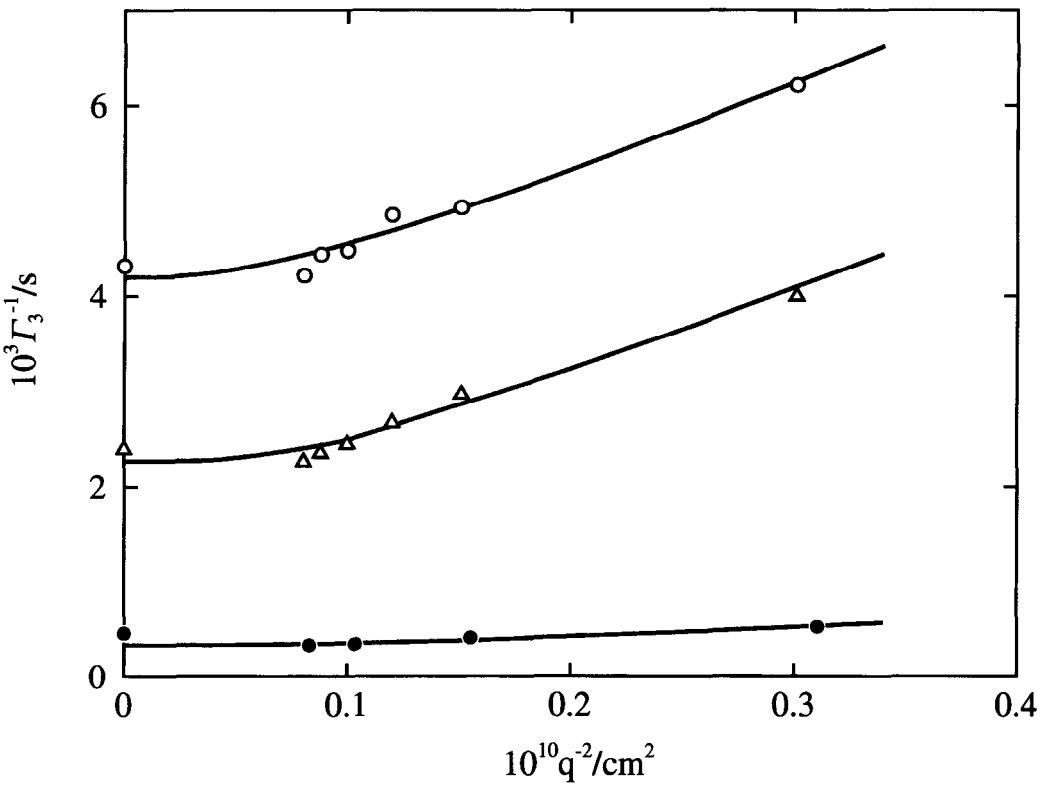

Fig. 12. Plots of Γ_3^{-1} against q^{-2} for solutions A (triangles), B (unfilled circles) and C (filled circles). The data points on the ordinate axis represent the values calculated by the first term of Eq. (31). The solid curves are merely to guide the eye.

Appendix A

Eq. (15) combined with Eqs. (10) and (16) yields

$$\hat{S}(q,\omega)=\frac{B(i\omega)}{A(i\omega)} \tag{A1}$$

where

$$A(i\omega)=(i\omega+Dq^2)\prod_{j=1}^{n}(i\omega+\tau_j^{-1}) + i\omega Cq^2\sum_{j=1}^{n}L_j\prod_{k=1(k\neq j)}^{n}(i\omega+\tau_k^{-1}) \tag{A2a}$$

$$B(i\omega)=\prod_{j=1}^{n}(i\omega+\tau_j^{-1})+Cq^2\sum_{j=1}^{n}L_j\prod_{k=1(k\neq j)}^{n}(i\omega+\tau_k^{-1}) \tag{A2b}$$

Eq. (A2a) indicates $A(i\omega)$ to be a polynomial of order $n+1$ in $(i\omega)$, and predicts that there are $n+1$ decay modes of $S(q,t)$ [30]. Thus, $\hat{S}(q,\omega)$ may be represented as

$$\hat{S}(q,\omega)=\sum_{j=1}^{n+1}\frac{r_j}{i\omega+\Gamma_j} \tag{A3a}$$

$$=\frac{\sum_{j=1}^{n+1}r_j\prod_{k=1(k\neq j)}^{n+1}(i\omega+\Gamma_k)}{\prod_{j=1}^{n+1}(i\omega+\Gamma_j)} \tag{A3b}$$

with

$$\sum_{j=1}^{n+1}r_j=1 \tag{A4}$$

Here, Γ_j and r_j are the decay rate and relative strength of the jth decay mode, and the subscript j is arranged so that $\Gamma_1<\Gamma_2<\Gamma_3<\cdots$. Inverse Fourier transformation of Eq. (A3a) gives

$$S(q,t)=\sum_{j=1}^{n+1}r_j e^{-\Gamma_j t} \tag{A5}$$

Eq. (18) in the text is the special case of this equation for $n=2$.

The root-coefficient relations for $A(i\omega)=0$ give

$$\sum_{j=1}^{n+1}\Gamma_j=D_cq^2+\sum_{j=1}^{n}\tau_j^{-1} \tag{A6}$$

$$\prod_{j=1}^{n+1}\Gamma_j=Dq^2\prod_{j=1}^{n}\tau_j^{-1} \tag{A7}$$

$$\sum_{j=1}^{n+1}\sum_{k=1}^{j-1}\Gamma_j\Gamma_k=\left[\sum_{j=1}^{n}\tau_j^{-1}+L_\pi^{-1}\sum_{j=1}^{n}L_j\sum_{k=1(k\neq j)}^{n}\tau_k^{-1}\right]Dq^2 + \sum_{j=1}^{n}\sum_{k=1}^{j-1}\tau_j^{-1}\tau_k^{-1} \tag{A8}$$

...

$$\sum_{j=1}^{n+1}\sum_{k=1(k\neq j)}^{n+1}\Gamma_k =\left[\sum_{j=1}^{n}\prod_{k=1(k\neq j)}^{n}\tau_k^{-1}+L_\pi^{-1}\sum_{j=1}^{n}L_j\prod_{k=1(k\neq j)}^{n}\tau_k^{-1}\right]Dq^2 + \prod_{j=1}^{n}\tau_j^{-1} \tag{A9}$$

Here, D_c is the cooperative diffusion coefficient defined by

$$D_c\equiv D+CL_0=C(L_\pi+L_0) \tag{A10}$$

with the instantaneous (on the DLS time scale) longitudinal modulus L_0 given by

$$L_0=\sum_{j=1}^{n}L_i \tag{A11}$$

The first cumulant K_1 for $S(q,t)$ is defined by

$$K_1=-[\partial\ln S(q,t)/\partial t]_{t\to 0} \tag{A12}$$

which, with Eq. (A5), gives

$$K_1=\sum_{j=1}^{n+1}r_j\Gamma_j \tag{A13}$$

Now, comparison of the coefficients of $(i\omega)^{n-1}$ in Eq. (A2b) and in the numerator of Eq. (A3b) gives

$$\sum_{j=1}^{n}\tau_j^{-1}+CL_0q^2=\sum_{j=1}^{n+1}r_j\sum_{k=1(k\neq j)}^{n+1}\Gamma_k \tag{A14}$$

which may be rewritten, with the aid of Eq. (A4), Eq. (A6) and Eq. (A10),

$$\sum_{j=1}^{n+1}r_j\Gamma_j=Dq^2 \tag{A15}$$

Hence, we have for arbitrary n

$$K_1=Dq^2 \tag{A16}$$

References

[1] Adam M, Delsanti M. J Phys Lett (Paris) 1984;45:L–279.
[2] Chen S-J, Berry GC. Polymer 1990;31:793.
[3] Nicolai T, Brown W, Johnsen RMW, Štěpánek P. Macromolecules 1990;23:1165.
[4] Nicolai T, Brown W, Hvdt S, Heller K. Macromolecules 1990;23:5088.
[5] Wang CH, Zhang XQ. Macromolecules 1993;26:707.
[6] Brown W, Štěpánek P. Macromolecules 1993;26:6884.

[7] Brown W, Nicolai T. In: Brown W, editor Dynamic light scattering, chapter 6 Oxford, UK: Clarendon Press, 1993.
[8] Berry GC. Adv Polym Sci 1994;114:233.
[9] Koike A, Nemoto N, Inoue T, Osaki K. Macromolecules 1995;28:2339.
[10] Wang CH., Sun Z, Huang QR. J Chem Phys 1996;105:6052.
[11] Jian T, Vlassopoulos D, Fytas G, Pakula T, Brown W. Colloid Polym Sci 1996;274:1033.
[12] Nicolai T, Brown W. In: Light scattering, principles and development, chapter 5 Oxford, UK: Clarendon Press, 1996.
[13] Wang CH. J Chem Phys 1991;95:3788.
[14] Wang CH. J Chem Phys 1995;102:6537.
[15] Doi M, Onuki A. J Phys II (Paris) 1992;2:1631.
[16] Onuki A. J Non-Crystalline Solids 1994;172-174:1151.
[17] Sun Z, Wang CH. Macromolecules 1994;27:4840.
[18] Brown W, Štěpánek P. Macromolecules 1994;27:4842.
[19] Einaga Y, Fujita H. Polymer, in press.
[20] Wang CH. J Non-Equilib Thermodyn 1995;20:274.
[21] Tobolsky AV. Properties and structure of polymers New York: Wiley, 1960.
[22] Eichinger BE, Flory PJ. Trans Farad Soc 1968;64:2053.
[23] Berry GC, Fox TG. Adv Polym Sci 1968;5:261.
[24] Akasaka K, Nakamura Y, Norisuye T, Teramoto A. Polym J 1994;26:363.
[25] Akasaka K, Nakamura Y, Norisuye T, Teramoto A. Polym J 1994;26:1387.
[26] Provencher SW. Makromol Chem 1979;180:201.
[27] Livesey AK, Licinio P, Delaye M. J Chem Phys 1986;84:5102.
[28] Einaga Y, Osaki K, Kurata M, Tamura M. Macromolecules 1972;5:635.
[29] Fetters LJ, Lohse DJ, Richter D, Witten TA, Zirkel A. Macromolecules 1994;27:4639.
[30] Genz U. Macromolecules 1994;27:3501.